nanomaterials

MDPI

Article

Platinum and Iridium Oxide Co-modified TiO_2 Nanotubes Array Based Photoelectrochemical Sensors for Glutathione

Jing Tian [1], Peng Zhao [1], Shasha Zhang [1], Guona Huo [1], Zhaochen Suo [1], Zhao Yue [2,*], Shoumin Zhang [1], Weiping Huang [1] and Baolin Zhu [1,3,*]

1 College of Chemistry, The Key Laboratory of Advanced Energy Materials Chemistry (Ministry of Education), Tianjin Key Lab of Metal and Molecule-based Material Chemistry, Nankai University, Tianjin 300071, China; tianjingnk@nankai.edu.cn (J.T.); zhaopeng@nankai.edu.cn (P.Z.); 2120170933@mail.nankai.edu.cn (S.Z.); 15230153709@163.com (G.H.); zc.suo@mail.nankai.edu.cn (Z.S.); zhangsm@nankai.edu.cn (S.Z.); hwp914@nankai.edu.cn (W.H.)

2 Department of Microelectronics, Nankai University, Tianjin 300350, China

3 National Demonstration Center for Experimental Chemistry Education (Nankai University), Tianjin 300071, China

* Correspondence: yuezhao@nankai.edu.cn (Z.Y.); zhubaolin@nankai.edu.cn (B.Z.)

Received: 15 February 2020; Accepted: 10 March 2020; Published: 13 March 2020

Abstract: Oriented TiO_2 nanotubes, which are fabricated by anodic oxidation method, are prospective in photoelectrochemical analysis and sensors. In this work, Pt and IrO_2 co-modified TiO_2 nanotubes array was prepared via a two-step deposition process involving the photoreductive deposition of Pt and chemical deposition of IrO_2 on the oriented TiO_2 nanotubes. Due to the improved separation of photo-generated electrons and holes, Pt-IrO_2 co-modified TiO_2 nanotubes presented significantly higher PEC activity than pure TiO_2 nanotubes or mono-modified TiO_2 nanotubes. The PEC sensitivity of Pt-IrO_2 co-modified TiO_2 nanotubes for glutathione was also monitored and good sensitivity was observed.

Keywords: TiO_2 nanotubes array/Ti electrode; Pt; IrO_2; co-modification; photoelectrochemical sensor; glutathione

1. Introduction

Photoelectrochemical (PEC) detection is a rapidly developing technique, due to its characteristics of high sensitivity, fast response speed, and simple instrumentation [1–6], and attracts a lot of research attention for detection of biomolecules, such as NADH, glucose, and glutathione, which are closely related to many serious diseases [7]. In PEC biosensors, photocurrent is produced by the physical and chemical interactions between biomolecules; photoactive species are identified as detection signal. The relationship between the biomolecule concentrations and photocurrent provides the foundation for PEC sensors. This promising analytical technology relies intensively on photoelectrodes. Hence, the selection of a proper photoelectrode is critical.

Diverse nanomaterials, such as Au [8], ZnO [9,10], CdS [11,12], TiO_2 [13,14], and porphyrin [15,16], have been exploited as electrodes. Among them, TiO_2 nanomaterials have been widely investigated due to their high PEC activity, stable performance, good biological compatibility, and obvious surface effect [17–19]. TiO_2 nanotube arrays can be grown directly on Ti substrates (TiO_2NTs/Ti) by anodic oxidation, which are good candidates for PEC electrodes. For such electrodes, Ti substrates have superior performance of electronic conduction, stability, and exhibit excellent compatibility, which enable them to be excellent implantable devices [20]. In addition, the unique one-dimensional

nanostructure of TiO_2 nanotube arrays accelerates electron transport and shortens the transfer distance of photogenerated carriers [21]. The tubular structure of TiO_2NTs can also facilitate the high dispersion of modified components and adsorption of aimed biomolecules. However, the application of TiO_2 in PEC detection is limited by its wide band gap and fast recombination of photogenerated charges, which can lower the photoenergy conversion efficiency and sensitivity of PEC sensors. A typical method to solve these problems is modification the TiO_2 photoelectrode with noble metals [22–24] or metal oxides [25,26]. The presence of noble metal results in the formation of a Schottky barrier at the metal-semiconductor interface, which can reduce the recombination of photogenerated charges and promote the separation of photogenerated charge carriers [27–29]. For instance, He's group prepared Pt particles modified TiO_2 film, and the photocurrent of 3 wt% Pt modified TiO_2 film under UV irradiation was 1.5 times higher than that of bare TiO_2 film [30]. In contrast to Pt, IrO_2 can intercept photogenerated holes from semiconductors and mediate the hole transfer process [31,32]. The synergistic effect of Pt and IrO_2 has been reported by Yuan's group [33]. Pt functioned as an electron collector while IrO_2 functioned as a hole capture, which may have led to significant charge separation and increased photocatalytic activity.

Glutathione (γ-glutamyl-cysteinyl-glycine, GSH), an important tripeptide, plays a major role in many biological functions such as gene expression regulation, cell protection, immune regulation, enzyme activity, and metabolic regulation, etc. [34,35]. Cellular concentration of GSH is related to a variety of human diseases [34,36], and the detection of GSH is urgent because of its importance in physiological circumstances. In this paper, Pt and IrO_2 nanoparticles were loaded on TiO_2NTs/Ti electrodes to form a Pt-IrO_2/TiO_2NTs/Ti electrode as shown in Scheme 1, leading to a novel PEC biosensing platform, which was then applied for the biodetection of GSH. This biosensor showed good sensing performance of GSH with a rapid response. The functions of Pt and IrO_2 in this system were also explored.

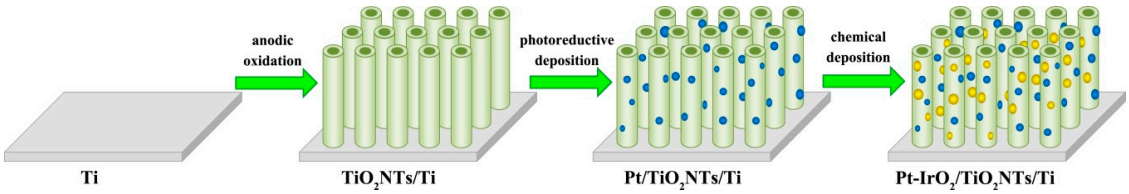

Scheme 1. Schematic representation of preparation process of Pt-IrO_2/TiO_2NTs/Ti electrode.

2. Experimental Section

2.1. Reagent and Apparatus

All chemical reagents were analytical grade and used without further purification. Reduced glutathione (GSH), PBS (0.1 M phosphate buffer, pH = 7.4 at 25 °C), $H_2IrCl_6 \cdot xH_2O$ and Ti foil were purchased from Sigma (Merck Life Science (Shanghai) Co., Ltd. Shanghai, China). $H_2PtCl_6 \cdot 4H_2O$ (Keruisi Chemical Reagent Co., Ltd. Tianjin, China) was used as platinum precursor. All aqueous solutions were prepared with 18 MΩ ultra purified water.

The chemical state of the elements on the photoelectrode was determined by Axis Ultra DLD multi-technique X-ray photoelectron spectrometer (Kratos Analytical Ltd., Manchester, UK). The phase structure of the catalysts was characterized by Rigaku D/Max-2500 X-ray diffractometer with Cu Kα radiation (Rigaku, Tokyo, Japan). Transmission electron microscopy (TEM) was performed using a Talos F200X G2 transmission electron microscope (FEI, Waltham, MA, USA). Scanning electron microscopy (SEM) was performed using a JSM-7500F scanning electron microscope (JEOL, Tokyo, Japan).

2.2. Preparation of TiO_2NTs/Ti

According to the reported anodic oxidation method [37,38], TiO_2 nanotubes arrays were prepared on Ti foil (30 mm × 10 mm × 0.127 mm). First, Ti foils were cleaned by sonicating in acetone, alcohol,

and deionized water for 15 min, respectively. Then they were etched in mixture liquor HF: HNO_3: H_2O = 1:4:5 for 30 s to remove the oxide layer. The prepared Ti foils were anodized by anodic inoxidation at 30 V for 6 h in an electrolytic solution (0.3 wt% NH_4F +2 vol% H_2O in ethylene glycol) under magnetic stirring at room temperature. The samples were sonicated for 15 min in ethanol and then dried in air. Finally, the as-prepared samples were calcinated at 400 °C for 2 h in a muffle furnace to obtain TiO_2NTs/Ti.

2.3. Preparation of Pt-IrO_2/TiO_2NTs/Ti

Pt-IrO_2/TiO_2NTs/Ti was prepared via a two-step deposition process involving the photoreductive deposition of Pt and chemical deposition of IrO_2 on TiO_2NTs/Ti. First, TiO_2NTs/Ti was dipped into a 0.05 mM H_2PtCl_6 solution (ethanol and deionized water with volume ratio 1:1) under the irradiation of 300 W UV light for 3 h to get the Pt modified TiO_2 nanotube array electrode (Pt/TiO_2NTs/Ti). Then, the Pt/TiO_2NTs/Ti was dipped into a 0.5 mM H_2IrCl_6 aqueous solution for 10 min, and dried in the oven at 150 °C for 10 min. After repeating the immersion process 5 times under the same conditions, the as-obtained sample was further annealed at 400 °C for 2 h to obtain Pt-IrO_2/TiO_2NTs/Ti. For comparation, IrO_2 modified TiO_2NTs (IrO_2/TiO_2NTs/Ti) were prepared by using TiO_2NTs/Ti as support.

2.4. Photoelectrochemical Measurement System

The photoelectrochemical experiments were performed with a CHI 604D electrochemical analyzer (CH Instruments, USA) using a three-electrode system. In the system, Ag/AgCl in 3 M KCl, platinum wire, and prepared electrodes were used as the reference electrode, counter electrode, and working electrode, respectively. An LED light source (M365L2: 365 nm, 90 mW) was fixed 30 cm above the working electrode and modulated by Transistor-Transistor Logic (TTL) out from a SR830 lock-in amplifier. PEC detection was carried out in PBS (pH = 7.4) containing different concentrations of GSH at room temperature. The switching on and off of the light source was controlled manually.

3. Results and Discussions

3.1. Microstructure Analysis

The XRD patterns of Ti foil, bare TiO_2NTs, and the modified TiO_2NTs/Ti are shown in Figure 1. The characteristic peaks of Ti (JCPDS# 44-1294) emerged in all patterns, because Ti foils were substrates. The peaks appearing at 25.28°, 37.80°, 48.05°, 53.89°, 55.06°, 62.69° observed in Figure 1b–e correspond to the diffraction of (101), (004), (200), (105), (211), (204) crystal planes of anatase TiO_2 (JCPDS# 21-1272), respectively. However, diffraction peaks of Pt or IrO_2 were not observed in the modified electrodes, which should be attributed to their high dispersion and low content.

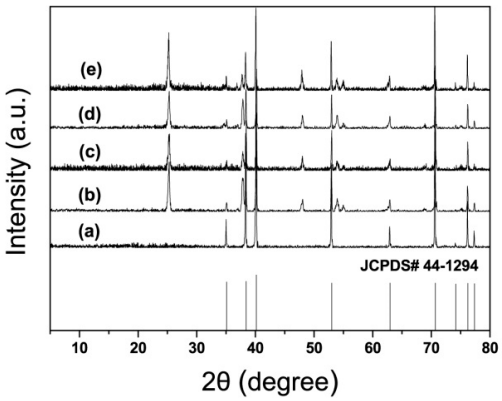

Figure 1. XRD patterns of (**a**) Ti foil; (**b**) TiO_2NTs/Ti; (**c**) Pt/TiO_2NTs/Ti; (**d**) IrO_2/TiO_2NTs/Ti; (**e**) Pt-IrO_2/TiO_2NTs/Ti.

The morphology and microstructure of the as-prepared TiO_2NTs/Ti was characterized by SEM and the Pt-IrO_2/TiO_2NTs/Ti was characterized by TEM. The top view SEM image (Figure 2a) shows that the bare TiO_2 nanotubes were highly ordered, with an average diameter of 80 nm and wall thickness of 18 nm. It is also clearly observed that the tubes were open on the top.

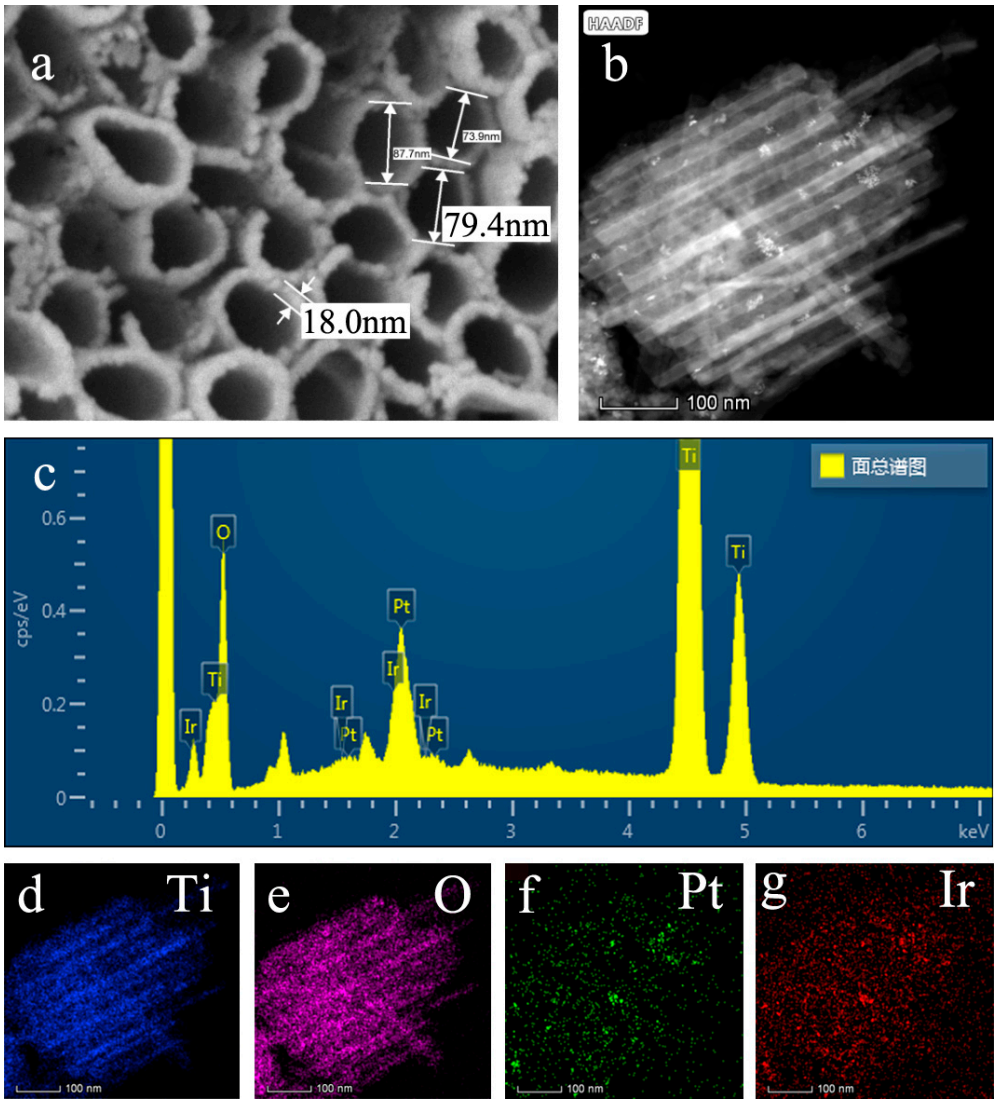

Figure 2. (**a**) Top-view SEM of TiO_2NTs; (**b**) The TEM image of Pt-IrO_2/TiO_2NTs/Ti; (**c**) The EDS of Pt-IrO_2/TiO_2NTs/Ti; (**d**–**g**) The EDS mappings of Pt-IrO_2/TiO_2NTs/Ti.

Figure 2b shows the microstructure of TiO_2NTs modified with Pt and IrO_2. To confirm the presence of Pt and IrO_2 on the TiO_2NTs, EDS and elemental mapping were carried out. The EDS (Figure 2c) showed that atomic percentages of Pt and Ir in Pt-IrO_2/TiO_2NTs/Ti were 0.70% and 0.41%, respectively. The elemental mappings present the existence of Pt and IrO_2 visually, as shown in Figure 2d–g. It can observe that the distributed Pt and Ir elements were homogeneous.

To further investigate the composition and elemental valences of the modified electrode, XPS analysis was performed. Figure 3 shows the XPS spectrum of Pt-IrO_2/TiO_2NTs/Ti, and corresponding high-resolution spectra of Ti2p, O1s, Pt4f, and Ir4f (Figure 3b–e). Figure 3a shows that the sample contained Ti, O, Pt and Ir, indicating successful deposition of Pt and IrO_2 on the TiO_2NTs, consistent with the EDS results. In Figure 3b, two peaks at BE of 464.0 eV and 458.5 eV in Pt-IrO_2/TiO_2NTs/Ti were assigned to $Ti2p_{1/2}$ and $Ti2p_{3/2}$ respectively, indicating the existence of Ti^{4+} in TiO_2 [14,39,40]. In Figure 3c, the peak at BE of 529.5 eV was assigned to Ti-O [41].

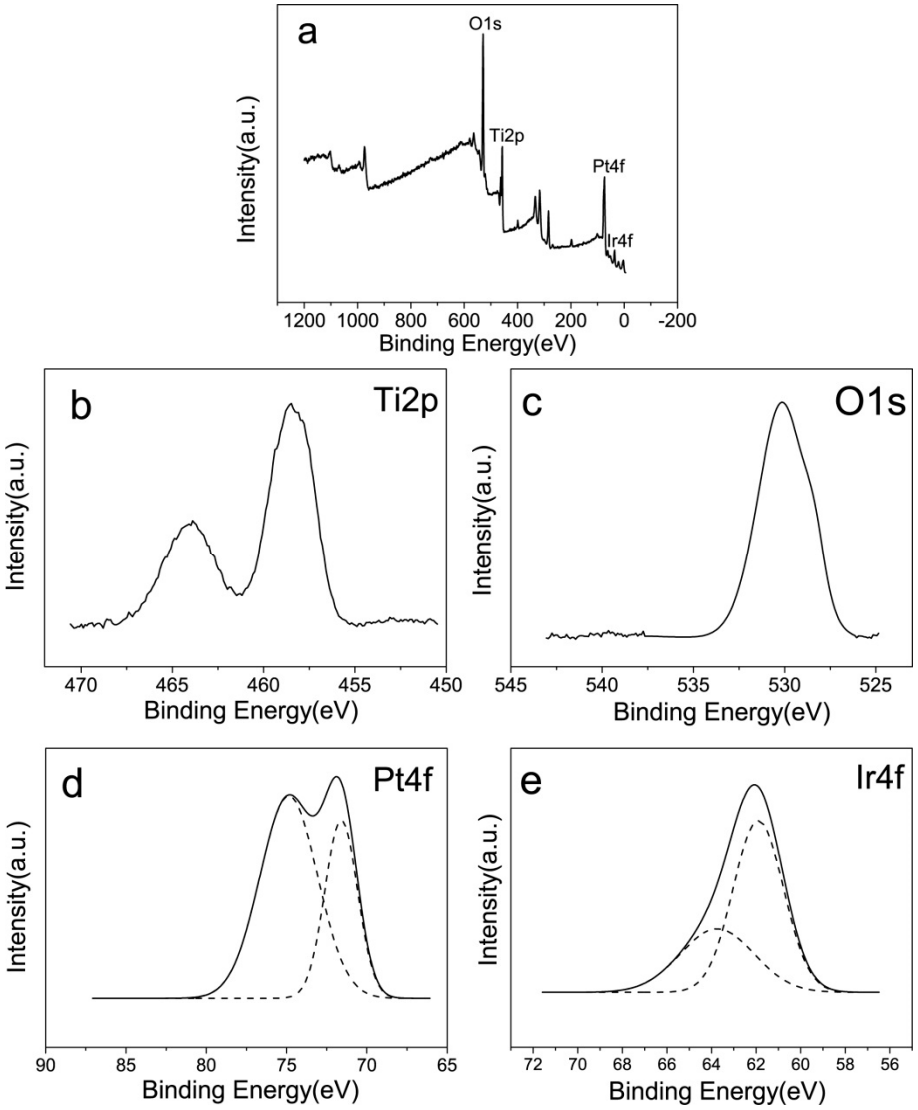

Figure 3. (**a**) XPS spectra of Pt-IrO_2/TiO_2NTs/Ti, (**b**) Ti2p, (**c**) O1s, (**d**) Pt4f; (**e**) Ir4f.

As displayed in Figure 3d, the satellite peaks at 75.0 eV and 71.6 eV are strong evidence for $Pt4f_{5/2}$ and $Pt4f_{7/2}$, which confirms the formation of metallic Pt after the photoreduction deposition process [42,43]. After deconvolution, the high-resolution Ir4f (Figure 3d) showed the peak at 64.9 eV for $Ir4f_{5/2}$ and 62.0 eV for $Ir4f_{7/2}$, which is the characteristic of Ir^{4+} in IrO_2 [41,44,45]. Consequently, Pt and IrO_2 were successfully deposited on the TiO_2NTs/Ti electrode, and Pt-IrO_2 co-modified electrode was fabricated.

3.2. *Photoelectrochemical Performance*

A photocurrent-time curve can be used to characterize the separation effect of photogenerated carriers, and the increase of photocurrent indicates the low recombination probability of photogenerated electron-holes. Figure 4 shows the photocurrent-time curves of different electrodes in 0.1 M PBS solution under 365 nm LED UV light irradiation. From Figure 4a, it can be seen that the photocurrent curve of the bare TiO_2NTs electrode had an anodic photocurrent spike at the initial time of irradiation, and then continuously decreased until a constant current was reached. However, the decorated TiO_2NTs electrodes could generate stable photocurrent more rapidly under the same condition, as shown in Figure 4b–d.

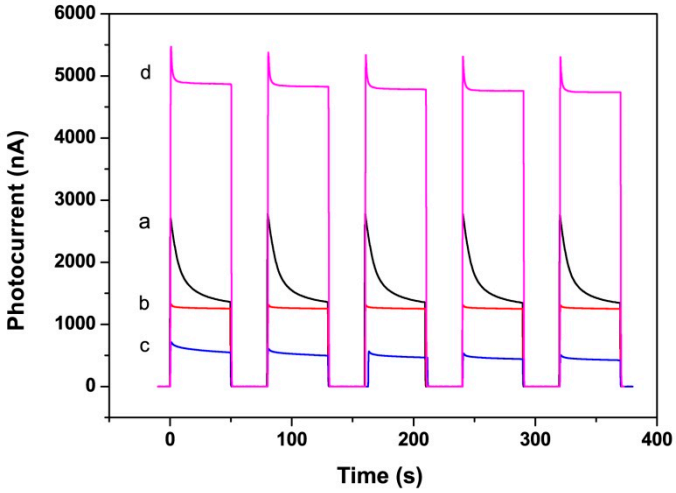

Figure 4. Photocurrent responses of different electrodes: (**a**) TiO_2NTs/Ti, (**b**) Pt/TiO_2NTs/Ti, (**c**) IrO_2/TiO_2NTs/Ti, (**d**) Pt-IrO_2/TiO_2NTs/Ti electrodes in 0.1M PBS solution under 365 nm LED irradiation.

Under illumination, TiO_2 could absorb UV light and generate electron-hole pairs, and electrons from the TiO_2 electrode could transfer to Pt. So the surface of Pt nanoparticles appeared negatively charged and TiO_2 appeared positively charged. The Schottky barrier prevents electrons from recombining with holes, and promotes the migration of charges, thus improves the stability of the photocurrent (Figure 4b). For IrO_2/TiO_2NTs/Ti, the photoinduced holes were taken by IrO_2, effectively preventing the combination of electron-hole. So the photocurrent of IrO_2/TiO_2NTs/Ti electrode also could quickly stabilize, as shown in Figure 4c. In the Pt-IrO_2 modified TiO_2 system, due to the synergistic effect of Pt and IrO_2, the recombination of photogenerated electrons and holes could be effectively blocked. The Pt-IrO_2/TiO_2NTs/Ti electrode in Figure 4d exhibited an apparent and stable photocurrent signal compared with the TiO_2NTs/Ti.

However, the mono Pt- or IrO_2-modified TiO_2NTs/Ti exhibited lower photocurrent responses than bare TiO_2NTs/Ti. The reason may be that Pt- and IrO_2-loading on TiO_2NTs shelter the TiO_2NTs from the light illumination, which could reduce the efficiency of photogenerated carriers. Another reason may be that when Pt or IrO_2 nanoparticles appeared alone on the TiO_2, both photogenerated electrons and holes may transfer to Pt or IrO_2 nanoparticles, making them act as recombination centers [46,47]. However, if Pt and IrO_2 nanoparticles co-exist, electrons would move to Pt, while holes move to IrO_2. The electron-hole recombination would be suppressed, leading to a higher photocurrent.

3.3. PEC biosensing Application for GSH

On the basis of photoelectrochemical performance, the application of the fabricated Pt-IrO_2/TiO_2NTs/Ti for detection of GSH was investigated. The electrode was kept in PBS at +0.3 V bias voltage under UV illumination for 5 min as pretreatment, and then the positive photocurrent was detected in the presence of GSH in PBS. As shown in Figure 5, the photocurrent increased with the addition of GSH under illumination, fitted with the Langmuir curve. The inset presented in Figure 5 shows that the photocurrent response of the Pt-IrO_2/TiO_2NTs/Ti biosensor was proportional to GSH concentration in the range of 1~10 μM with the regression equation of $I\text{-}I_0(\mu A) = 2.505 + 54.171C_{GSH}(uM)$ (R^2 = 0.9932) (I represents the photocurrent obtained in the presence of GSH, and I_0 is the blank photocurrent). The detection limit (LOD) of the sensor can be obtained from the formula LOD = 3 Sb/S (Sb = standard deviation of blank signal, S = sensitivity), and the calculated value was 0.8 μM.

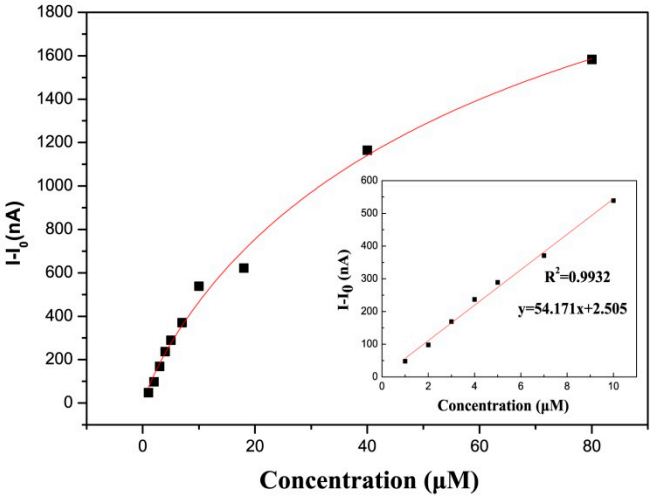

Figure 5. The curve of Pt-IrO_2/TiO_2NTs/Ti for the detection of different concentrations for GSH.

Scheme 2 illustrates the PEC process for GSH detection by Pt-IrO_2/TiO_2NTs/Ti biosensor. Under the illumination of UV light, electron-hole pairs were generated in TiO_2. Due to the Schottky barrier at the Pt/TiO_2 interface, electrons moved from TiO_2 electrode to Pt. Simultaneously, the photoinduced holes were taken by IrO_2, and then oxidized GSH to GSSG.

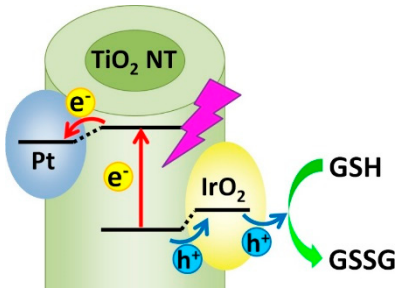

Scheme 2. Schematic illustration of the PEC process for GSH detection by Pt-IrO_2/TiO_2NTs/Ti biosensor.

Table 1 summarizes the comparison of analytical performance of various GSH biosensors. The Pt-IrO_2/TiO_2NTs/Ti biosensor had a relatively reasonable linear range in 1-10 μM. Compared with other non-enzymatic sensors, Pt-IrO_2/TiO_2NTs/Ti was sensitive and could be used at relatively low GSH concentrations. Though enzymatic sensors offer high sensitivity, non-enzymatic sensors are widely recognized for their good advantages of simple operation, lack of need for expensive equipment, and high stability. The stability of the Pt-IrO_2/TiO_2NTs biosensor was tested by measuring photocurrent response after 30 days (see Supplementary Figure S1). The photocurrent did not decrease significantly, indicating that the electrode's good stability for GSH detection. This should contribute to the good stability of Pt and IrO_2 on TiO_2NTs/Ti electrodes.

Table 1. Comparison of various GSH sensors.

	GSH Biosensor	Linear Range (μM)	Detection Limit (μM)	Ref.
Non-enzymatic sensor	Pt-IrO_2/TiO_2NTs/Ti	1–10	0.8	This work
	Cu_2O/ZnO	1–10 and 20–100	0.8	[48]
	GR-CdS/ITO	10–1500	3	[49]
	rGO/ZnO	10–200	2.17	[50]
	Porphyrin-Functionalized TiO_2-ITO	50–2400	30	[16]
Enzymatic sensor	IrO_2-Hemin-TiO_2 nanowire arrays	0.01–10	0.01	[17]

In summary, a PEC sensor for GSH was designed using Pt-IrO_2/TiO_2NTs/Ti as an electrode. Pt and IrO_2 were evenly distributed on TiO_2NTs/Ti. Due to the synergistic effects of Pt and IrO_2, the Pt-IrO_2/TiO_2NTs/Ti electrode exhibited an apparent and stable photocurrent signal compared with the TiO_2NTs/Ti or the mono-modified ones. The photocurrent signals of the Pt-IrO_2/TiO_2NT/Ti biosensor was linear to GSH concentration in the range of 1~10 μM. Other kinds of modified TiO_2NTs/Ti electrodes which may exhibit high PEC sensitivity under visible light are anticipated.

Supplementary Materials: The following are available online at http://www.mdpi.com/2079-4991/10/3/522/s1, Figure S1: The curve of Pt-IrO_2/TiO_2NTs/Ti (after 30 days) for the detection of different concentrations for GSH.

Author Contributions: All authors have participated actively in the development of this work. J.T. and B.Z. conceived and designed the experiments; J.T. performed the experiments; J.T., Z.Y., S.Z. (Shoumin Zhang), W.H., and B.Z. analyzed the data; P.Z. contributed analysis tools; S.Z. (Shasha Zhang), G.H., and Z.S. contributed reagents; J.T. wrote the paper. All authors have read and agreed to the published version of the manuscript.

Funding: This research was funded by the National Natural Science Foundation of China (Nos. 61471207 and 61871240).

Conflicts of Interest: The authors declare no conflict of interest.

References

1. Zhang, J.; Tu, L.; Zhao, S.; Liu, G.; Wang, Y.; Wang, Y.; Yue, Z. Fluorescent gold nanoclusters based photoelectrochemical sensors for detection of H_2O_2 and glucose. *Biosens. Bioelectron.* **2015**, *67*, 296–302. [CrossRef] [PubMed]
2. Zhang, N.; Ruan, Y.F.; Zhang, L.B.; Zhao, W.W.; Xu, J.J.; Chen, H.Y. Nanochannels photoelectrochemical biosensor. *Anal. Chem.* **2018**, *90*, 2341–2347. [CrossRef] [PubMed]
3. Yu, L.M.; Zhu, Y.C.; Liu, Y.L.; Qu, P.; Xu, M.T.; Shen, Q.; Zhao, W.W. Ferroelectric perovskite oxide@TiO_2 nanorod heterostructures: Preparation, characterization, and application as a platform for photoelectrochemical bioanalysis. *Anal. Chem.* **2018**, *90*, 10803–10811. [CrossRef] [PubMed]
4. Ruan, Y.F.; Zhang, N.; Zhu, Y.C.; Zhao, W.W.; Xu, J.J.; Chen, H.Y. Photoelectrochemical bioanalysis platform of gold nanoparticles equipped perovskite Bi_4NbO_8Cl. *Anal. Chem.* **2017**, *89*, 7869–7875. [CrossRef]
5. Li, Y.; Zhang, N.; Zhao, W.W.; Jiang, D.C.; Xu, J.J.; Chen, H.Y. Polymer dots for photoelectrochemical bioanalysis. *Anal. Chem.* **2017**, *89*, 4945–4950. [CrossRef]
6. Tu, L.; Liu, G.; Zhang, W.; Qin, J.; Yue, Z. Doped QDs based photoelectrochemical sensors for detection of H_2O_2 and Glucose. *IEEE J. Sel. Top. Quantum.* **2014**, *20*, 175–183. [CrossRef]
7. Wu, S.; Song, H.; Song, J.; He, C.; Ni, J.; Zhao, Y.; Wang, X. Development of triphenylamine functional dye for selective photoelectrochemical sensing of cysteine. *Anal. Chem.* **2014**, *86*, 5922–5928. [CrossRef]
8. Tee, S.Y.; Ye, E.; Pan, P.H.; Lee, C.J.; Hui, H.K.; Zhang, S.Y.; Koh, L.D.; Dong, Z.; Han, M.Y. Fabrication of bimetallic Cu/Au nanotubes and their sensitive, selective, reproducible and reusable electrochemical sensing of glucose. *Nanoscale* **2015**, *7*, 11190–11198. [CrossRef]
9. Li, Y.; Zhang, X.; Jiang, S.; Dai, H.; Sun, X.; Li, Y. Improved photoelectrochemical property of a nanocomposite NiO/CdS@ZnO photoanode for water splitting. *Sol. Energy Mater. Sol. Cells* **2015**, *132*, 40–46. [CrossRef]
10. Wang, T.; Jin, B.; Jiao, Z.; Lu, G.; Ye, J.; Bi, Y. Electric field-directed growth and photoelectrochemical properties of cross-linked Au-ZnO hetero-nanowire arrays. *Chem. Commun.* **2015**, *51*, 2103–2106. [CrossRef]
11. Okoth, O.K.; Yan, K.; Feng, J.; Zhang, J. Label-free photoelectrochemical aptasensing of diclofenac based on gold nanoparticles and graphene-doped CdS. *Sens. Actuators B* **2018**, *256*, 334–341. [CrossRef]
12. Zhang, J.; Wang, L.; Liu, X.; Li, X.A.; Huang, W. High-performance CdS–ZnS core–shell nanorod array photoelectrode for photoelectrochemical hydrogen generation. *J. Mater. Chem. A* **2015**, *3*, 535–541. [CrossRef]
13. Zhu, J.; Huo, X.; Liu, X.; Ju, H. Gold nanoparticles deposited polyaniline-TiO_2 nanotube for surface plasmon resonance enhanced photoelectrochemical biosensing. *ACS Appl. Mater. Interfaces* **2016**, *8*, 341–349. [CrossRef] [PubMed]
14. Tao, J.; Gong, Z.; Yao, G.; Cheng, Y.; Zhang, M.; Lv, J.; Shi, S.; He, G.; Chen, X.; Sun, Z. Enhanced photocatalytic and photoelectrochemical properties of TiO_2 nanorod arrays sensitized with CdS nanoplates. *Ceram. Int.* **2016**, *42*, 11716–11723. [CrossRef]

15. Zhou, Y.; Shi, Y.; Wang, F.B.; Xia, X.H. Oriented self-assembled monolayer of Zn(II)-tetraphenylporphyrin on TiO_2 electrode for photoelectrochemical analysis. *Anal. Chem.* **2019**, *91*, 2759–2767. [CrossRef]
16. Tu, W.; Dong, Y.; Lei, J.; Ju, H. Low-potential photoelectrochemical biosensing using porphyrin-functionalized TiO_2 nanoparticles. *Anal. Chem.* **2010**, *82*, 8711–8716. [CrossRef]
17. Tang, J.; Kong, B.; Wang, Y.; Xu, M.; Wang, Y.; Wu, H.; Zheng, G. Photoelectrochemical detection of glutathione by IrO_2-hemin-TiO_2 nanowire arrays. *Nano Lett.* **2013**, *13*, 5350–5354. [CrossRef]
18. Chen, D.; Zhang, H.; Li, X.; Li, J. Biofunctional titania nanotubes for visible-light-activated photoelectrochemical biosensing. *Anal. Chem.* **2010**, *82*, 2253–2261. [CrossRef]
19. Singh, S.C.; Swarnkar, R.K.; Gopal, R. Synthesis of Titanium Dioxide Nanomaterial by Pulsed Laser Ablation in Water. *J. Nanosci. Nanotechnol.* **2009**, *9*, 5367–5371. [CrossRef]
20. Prasad, K.; Bazaka, O.; Chua, M.; Rochford, M.; Fedrick, L.; Spoor, J.; Symes, R.; Tieppo, M.; Collins, C.; Cao, A.; et al. Metallic biomaterials: Current challenges and opportunities. *Materials* **2017**, *10*, 884. [CrossRef]
21. Wang, L.; Han, J.; Feng, J.; Wang, X.; Su, D.; Hou, X.; Hou, J.; Liang, J.; Dou, S.X. Simultaneously efficient light absorption and charge transport of CdS/TiO_2 nanotube array toward improved photoelectrochemical performance. *Int. J. Hydrogen Energy* **2019**, *44*, 30899–30909. [CrossRef]
22. Subramanian, V.; Wolf, E.; Kamat, P.V. Semiconductor-Metal composite nanostructures. To what extent do metal nanoparticles improve the photocatalytic activity of TiO_2 films? *J. Phys. Chem. B* **2001**, *105*, 11439–11446. [CrossRef]
23. Zhang, Z.; Wang, Z.; Cao, S.-W.; Xue, C. Au/Pt nanoparticle-decorated TiO_2 nanofibers with plasmon-enhanced photocatalytic activities for solar-to-fuel conversion. *J. Phys. Chem. C* **2013**, *117*, 25939–25947. [CrossRef]
24. Chandrasekharan, N.; Kamat, P.V. Improving the photoelectrochemical performance of nanostructured TiO_2 films by adsorption of gold nanoparticles. *J. Phys. Chem. B* **2000**, *104*, 10851–10857. [CrossRef]
25. Akita, A.; Kobayashi, H.; Tada, H. Ultrathin Silicon Oxide film-induced enhancement of charge separation and transport of nanostructured Titanium(IV) Oxide photoelectrode. *Chemphyschem* **2019**, *20*, 2054–2059. [CrossRef]
26. Wang, M.; Sun, L.; Lin, Z.; Cai, J.; Xie, K.; Lin, C. p–n Heterojunction photoelectrodes composed of Cu_2O-loaded TiO_2 nanotube arrays with enhanced photoelectrochemical and photoelectrocatalytic activities. *Energy Environ. Sci.* **2013**, *6*, 1211–1220. [CrossRef]
27. Ji, L.; Spanu, D.; Denisov, N.; Recchia, S.; Schmuki, P.; Altomare, M. A dewetted-dealloyed nanoporous Pt co-catalyst formed on TiO_2 nanotube arrays leads to strongly enhanced photocatalytic H_2 production. *Chem. Asian J.* **2019**. [CrossRef]
28. Linsebigler, A.L.; Lu, G.; Yates, J.T. Photocatalysis on TiO_2 surfaces: Principles, mechanisms, and selected results. *Chem. Rev.* **1995**, *95*, 735–758. [CrossRef]
29. Li, X.Z.; Li, F.B. Study of Au/Au^{3+}-TiO_2 photocatalysts toward visible photooxidation for water and waste water treatment. *Environ. Sci. Technol.* **2001**, *35*, 2381–2387. [CrossRef]
30. Guo, Y.; He, J.; Wu, S.; Wang, T.; Li, G.; Hu, Y.; Xue, H.; Sun, X.; Tang, J.; Liu, M. Effects of platinum on photo-assisted electrocatalytic activity of fringe-shaped highly ordered mesoporous titanium dioxide film. *J. Power Sources* **2012**, *208*, 58–66. [CrossRef]
31. Meekins, B.H.; Kamat, P.V. Role of water oxidation catalyst IrO_2 in shuttling photogenerated holes across TiO_2 interface. *J. Phys. Chem. Lett.* **2011**, *2*, 2304–2310. [CrossRef]
32. Kamat, P.V. Manipulation of charge transfer across semiconductor interface. A criterion that cannot be ignored in photocatalyst design. *J. Phys. Chem. Lett.* **2012**, *3*, 663–672. [CrossRef] [PubMed]
33. Wang, D.; Wang, W.; Wang, Q.; Guo, Z.; Yuan, W. Spatial separation of Pt and IrO_2 cocatalysts on SiC surface for enhanced photocatalysis. *Mater. Lett.* **2017**, *201*, 114–117. [CrossRef]
34. Li, X.; Xu, Y.; Chen, Y.; Wang, C.; Jiang, J.; Dong, J.; Yan, H.; Du, X. Dual enhanced electrochemiluminescence of aminated Au@SiO_2/CdS quantum dot superstructures: Electromagnetic field enhancement and chemical enhancement. *ACS Appl. Mater. Interfaces* **2019**, *11*, 4488–4499. [CrossRef] [PubMed]
35. Sui, M.; Zhao, Y.; Ni, Z.; Gu, X. Photoelectrochemical performance and biosensor application for glutathione (GSH) of W-doped $BiVO_4$ thin films. *J. Mater. Sci. Mater. Electron* **2018**, *29*, 10109–10116. [CrossRef]
36. Li, Z.; Zhang, J.; Li, Y.; Zhao, S.; Zhang, P.; Zhang, Y.; Bi, J.; Liu, G.; Yue, Z. Carbon dots based photoelectrochemical sensors for ultrasensitive detection of glutathione and its applications in probing of myocardial infarction. *Biosens. Bioelectron.* **2018**, *99*, 251–258. [CrossRef]

37. Prakasam, H.E.; Shankar, K.; Paulose, M.; Varghese, O.K.; Grimes, C.A. A new benchmark for TiO_2 nanotube array growth by anodization. *J. Phys. Chem. C* **2007**, *111*, 7235–7241. [CrossRef]
38. Li, W.; Kuang, D.; Gu, P.; Xiang, M. Partially disordered TiO_2 nanotube photonic crystal: Randomness characterization and tuning of reflected scattering light. *Nanotechnology* **2020**, *31*, 025711. [CrossRef]
39. Zhou, H.; Zhang, Y. Electrochemically self-doped TiO_2 nanotube arrays for supercapacitors. *J. Phys. Chem. C* **2014**, *118*, 5626–5636. [CrossRef]
40. Zhang, R.; Ren, X.; Shi, X.; Xie, F.; Zheng, B.; Guo, X.; Sun, X. Enabling Effective Electrocatalytic N_2 Conversion to NH_3 by the TiO_2 Nanosheets Array under Ambient Conditions. *ACS Appl. Mater. Interfaces* **2018**, *10*, 28251–28255. [CrossRef]
41. Abb, M.J.S.; Weber, T.; Glatthaar, L.; Over, H. Growth of ultrathin single-crystalline IrO_2(110) films on a TiO_2(110) single crystal. *Langmuir* **2019**, *35*, 7720–7726. [CrossRef] [PubMed]
42. Vovk, E.I.; Kalinkin, A.V.; Smirnov, M.Y.; Klembovskii, I.O.; Bukhtiyarov, V.I. XPS study of stability and reactivity of oxidized Pt nanoparticles supported on TiO_2. *J. Phys. Chem. C* **2017**, *121*, 17297–17304. [CrossRef]
43. Liang, Y.; Ding, M.; Yang, Y.; Xu, K.; Luo, X.; Yu, T.; Zhang, W.; Liu, W.; Yuan, C. Highly dispersed Pt nanoparticles on hierarchical titania nanoflowers with {010} facets for gas sensing and photocatalysis. *J. Mater. Sci.* **2019**, *54*, 6826–6840. [CrossRef]
44. Chung, W.-H.; Tsai, D.-S.; Fan, L.-J.; Yang, Y.-W.; Huang, Y.-S. Surface oxides of Ir(111) prepared by gas-phase oxygen atoms. *Surf. Sci.* **2012**, *606*, 1965–1971. [CrossRef]
45. Chakrapani, K.; Sampath, S. The dual role of borohydride depending on reaction temperature: Synthesis of iridium and iridium oxide. *Chem. Commun.* **2015**, *51*, 9690–9693. [CrossRef]
46. Wang, W.N.; An, W.J.; Ramalingam, B.; Mukherjee, S.; Niedzwiedzki, D.M.; Gangopadhyay, S.; Biswas, P. Size and structure matter: Enhanced CO_2 photoreduction efficiency by size-resolved ultrafine Pt nanoparticles on TiO_2 single crystals. *J. Am. Chem. Soc.* **2012**, *134*, 11276–11281. [CrossRef]
47. Swierk, J.R.; McCool, N.S.; Saunders, T.P.; Barber, G.D.; Strayer, M.E.; Vargas-Barbosa, N.M.; Mallouk, T.E. Photovoltage Effects of Sintered IrO_2 Nanoparticle Catalysts in Water-Splitting Dye-Sensitized Photoelectrochemical Cells. *J. Phys. Chem. C* **2014**, *118*, 17046–17053. [CrossRef]
48. Li, J.; Li, H.; Xue, Y.; Fang, H.; Wang, W. Facile electrodeposition of environment-friendly Cu_2O/ZnO heterojunction for robust photoelectrochemical biosensing. *Sens. Actuators B* **2014**, *191*, 619–624. [CrossRef]
49. Zhao, X.; Zhou, S.; Shen, Q.; Jiang, L.P.; Zhu, J.J. Fabrication of glutathione photoelectrochemical biosensor using graphene-CdS nanocomposites. *Analyst* **2012**, *137*, 3697–3703. [CrossRef] [PubMed]
50. Kang, Z.; Gu, Y.; Yan, X.; Bai, Z.; Liu, Y.; Liu, S.; Zhang, X.; Zhang, Z.; Zhang, X.; Zhang, Y. Enhanced photoelectrochemical property of ZnO nanorods array synthesized on reduced graphene oxide for self-powered biosensing application. *Biosens. Bioelectron.* **2015**, *64*, 499–504. [CrossRef] [PubMed]

© 2020 by the authors. Licensee MDPI, Basel, Switzerland. This article is an open access article distributed under the terms and conditions of the Creative Commons Attribution (CC BY) license (http://creativecommons.org/licenses/by/4.0/).